Graph Construction for Uncrewed Convertiplanes Incorporating Operational Risk Using Geospatial Data

Philipp Hermann Müller, Florian Knaak, Rafael Godinho Ferreira, Nicolai Voget, and Dieter Moormann[1]

***Abstract*—The increasing use of Uncrewed Aircraft Vehicles (UAV) over populated areas creates the need for path planning methods that reduce both the ground and air risk caused by these operations. Risk calculation is especially challenging for the use of convertiplanes, which combine the ability to take-off and land vertically with the ability of fast wingborne flight due to their possibility to significantly vary speed during flight. As flight speed is a key factor to risk, both geospatial information and UAV parameters need to be incorporated into the planning process. For risk-aware flight path planning in large areas we employ the Probabilistic Roadmap (PRM) algorithm. This paper describes the graph generation process of a PRM algorithm that considers both ground and air risk based on the Specific Operations Risk Assessment (SORA) 2.5 approach taking into account varying flight speeds. The graph generation consists of the sampling and connection phases. During the connection phase the flight dynamic limitations of the UAV are taken into account. Finally, the presented process is demonstrated for Aachen.**

***Index Terms*—convertiplane, graph, operational risk, SORA, UAV**

I. Introduction

The use of Uncrewed Aerial Vehicles over longer distances, e.g. to transport urgent medical goods, is investigated in the Interreg project EDEN-Medical [1]. For these operations convertiplanes are well-suited as they combine the possibility of taking off and landing vertically (VTOL capability) with the capability to fly efficiently at high speeds over long distances, which increases their operational range significantly. Everyday applications require an efficient way to plan flight paths in often densely populates areas. Here, operational risk must be taken into account.

As summarized by Du et al. in [2] several approaches for risk aware flight planning exist. Due to the large areas covered in operations Beyond Visual Line Of Sight (BVLOS), existing approaches rely on sampling-based approaches such as rapidly-exploring random tree (RRT) or Probabilistic Roadmap (PRM) [3], [4]. However, air risk is typically neglected as the probability of conflicts with the current air traffic is considered to be low [5]. When quantifying the operational risk, assessment is often limited to one single speed and a single aircraft configuration (e.g. in [3]). This approach has to be expanded for convertiplanes, as they can operate in a large speed range from hover flight to fast cruise flight.

Speed substantially affects both air and ground risk in the safety assessment required to achieve a operating permit within the European Union (EU). This process is laid out in *Implementing Regulation (EU) 2019/947* [6] and is described in more detail in the *EASY Access Rules* [7].

PRM based path planning requires a graph. This paper presents a framework to build a risk-aware graph for convertiplanes, using the Probabilistic Roadmap (PRM) approach. It will be assumed that, except for obstacles, the UAV is allowed to move freely in the given area. The objective of the graph is to make it possible to plan a path that minimizes the operational risk of the flight operation between two points in the flight area.

The remainder of this paper is structured into four chapters. In the following chapter, existing methods will be examined. Chapter III will present the new approach of this paper: creating risk-aware graphs for convertiplanes at different flight speeds. Chapter IV will present and discuss the results of applying this approach to Aachen for different PRM variants. Finally, the results will be summarized in chapter V.

II. Methodical background

The first part of this chapter describes the used risk assessment model while the second part presents different PRM algorithms.

A. Risk Assessment Model

This paper uses the risk model introduced by the Joint Authorities for Rulemaking on Unmanned Systems (JARUS) in the SORA Framework. Here, the ground risk class (GRC) and the air risk class (ARC) are combined to determine the overall risk indicator called Specific Assurance and Integrity Level (SAIL). The combination of GRC and ARC is done via the SAIL determination table found in [7]. Optional mitigations and further steps after the risk combination will not be performed in the context of this paper.

GRC is based on the population density, ARC is determined by the airspace category. Additionally, both depend on the volume in which the UAV is operated. To determine the GRC and the ARC the affected volumes are calculated. The affected volume is divided into the Flight Geography (FG),

[1]All authors are with the Institute of Flight System Dynamics, RWTH Aachen University, 52056 Aachen, Germany. philipp.mueller@fsd.rwth-aachen.de

Acknowledgement: The EDEN-Medical project is supported by the European Union and the Interreg Meuse-Rhine (NL-BE-DE) programme. Cofinancing is provided by the Ministry of Economic Affairs, Industry, Climate Action and Energy of the State of North Rhine-Westphalia (DE) and the Province of Limburg (NL).

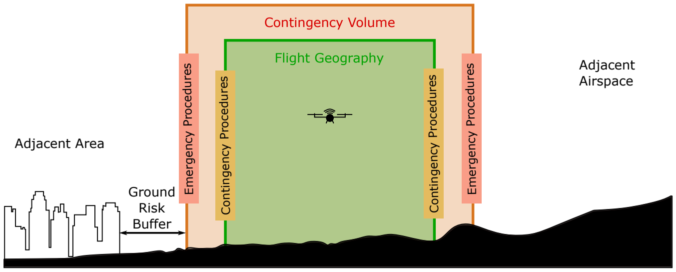

Fig. 1: Operational Volume according to [7]

the Contingency Volume (CV) and the Ground Risk Buffer (GRB). A graphical representation is given in Figure 1.

The size of the volumes is strongly influenced by the speed and type of UAV being used, as different calculations have to be applied depending on the UAV configuration. This is particularly noteworthy for convertiplanes as they can transition between configurations mid-flight. The guidelines for those calculations are laid out in Annex A of SORA 2.5 [8]. For determining the GRB this paper will consider both the ballistic approach and the 1:1 rule. The ballistic approach is applied when the convertiplane is in multirotor mode while the 1:1 rule is used when in fixed wing-flight. The size of the GRB differs significantly based on the used approach. Computing the CV is based on SORA guidelines with adaptions for the reference aircraft as detailed in [9].

B. PRM-Based Planning Algorithms

This paper uses the PRM approach, which was first presented in [10] and can be split into three phases, namely sampling phase, connection phase, and query phase. In the sampling phase, the area to be considered (configuration space) is randomly sampled. All collision free samples become nodes of the graph. Thereafter, neighbouring nodes get connected. Variations of PRM such as k-PRM* and PRM* mainly differ in their implementation of this connection phase[11].

The k-PRM* algorithm, proposed by Karaman and Frazzoli [11], is a variation of the k-nearest neighbour PRM algorithm, which connects the k-nearest neighbours to a node. Whereas the number of neighbours is fixed independent of the number of nodes for the k-nearest PRM algorithm, the k-PRM* algorithm determines this number based on the overall number of nodes and the dimension of the sampled space.

Unlike the k-PRM* algorithm that doesn't take into account the distance of the neighbours from the node, the PRM* algorithm determines a uniform connection radius based on the number of nodes and the dimension of the sampled space [11]. The PRM* algorithm only connects each node only with neighbours within the connection radius.

All connections identified during the connection phase that do not collide with the terrain, the border of the area of operation and obstacles are stored as a graph. In the following query phase this graph can then be repeatedly used for any number of path finding queries as long as the underlying data remain unchanged. The implementation of the graph search algorithm for the query phase is not part of this paper.

III. Implementation

This chapter is divided into three sections. The first section describes the preprocessing necessary before the graph creation. Section III-B will focus on the sampling approach used. The connection phase is then explained in Section III-C.

The process of creating the graph from geospatial data is outlined in figure 2. This paper will follow the SORA approach of computing the risk based on population density and airspace category. The necessary information will be extracted from readily available open source data. On the right hand side of the figure the type of data used can be seen, shown as ellipses. On the left hand side the necessary steps to create the graph are shown. Input and output objects are shown as rectangles with rounded edges, while actions are symbolized by hexagons. The process starts by randomly sampling the area of operation, where samples within obstacles get discarded right away. For each node, GRC and ARC are determined based on the population density in the affected area and the airspaces above the affected area, respectively. GRC and ARC are combined to retrieve the corresponding SAIL. During the following connection process only connections free from collisions with obstacles and the terrain are saved as edges of the graph. The SAIL determination process is performed for each edge.

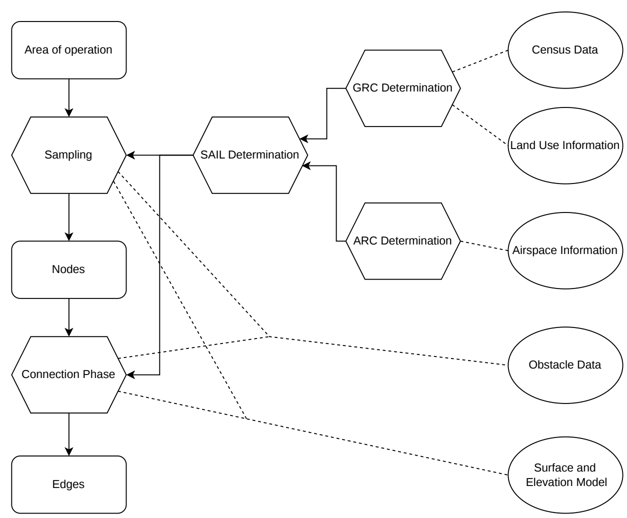

Fig. 2: Graph creation process

A. Preprocessing

Different types of geospatial information need to be processed to determine both the GRC and the ARC. The used sources of geospatial data are summarized in table I. The reliability of the risk assessment heavily depends on the quality of the available data sources used to identify the population density and the air space type.

TABLE I: Overview of used data sources

Name	Description	Source
OpenStreetMap (OSM)	Open source data for streets, buildings etc.	[12]
JRC-CENSUS population grid 2021	Residential population counts for Europe according to the 2021 census, resolution of $100 \times 100\,\mathrm{m}^2$ cells	[13]
NASADEM Global Digital Elevation Model	Digital Elevation Model	[14]
European Digital Elevation Model (EU-DEM)	Digital Surface Model	[15]
OpenAip	Airspace Information (e.g. TMZ, CTR, ED-R)	[16]
LUISA Base Map 2018	High-resolution land use/land cover map	[17]

To improve the representation of the distribution of the population, land use information is combined with census data according to the guidelines provided by EASA in [18]. The resulting population density map has a resolution of $200 \times 200\,\mathrm{m}^2$.

The airspace information is filtered by the height of the Contingency Volume, allowing only relevant airspaces to be considered for ARC determination.

The width of the Flight Geography of each edge has to be chosen such that a UAV remains inside during a turn to the following edge element. This width is determined by the cross-track deviation d during the turn from the line of sight connecting the nodes of the edge, see figure 3. The cross-track deviation can be calculated with equation 1 where $R_{\min}$ is the minimal turning radius of the aircraft and $\Delta\chi$ is the enclosed angle as shown in figure 3.

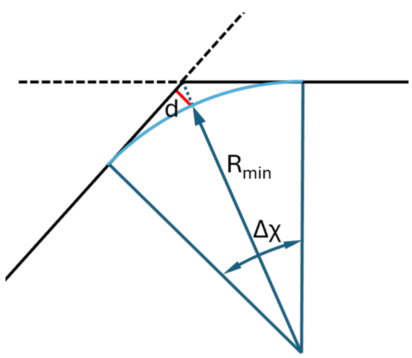

Fig. 3: Cross-track deviation from line of sight

$$d = R_{\min} \cdot \left[1 - \cos\left(\frac{\Delta\chi}{2}\right)\right] \quad (1)$$

The minium turning radius $R_{\min}$ of the UAV is calculated using equation 2 where g is the gravitational acceleration, V the flight speed and Φ the bank angle. Using $\Phi = \Phi_{\max}$ gives the minium turning radius. This equation is used both for multirotor and fixed-wing configuration as a conservative estimate.

$$R_{\min} = \frac{V^2}{g \cdot \tan(\Phi_{\max})} \quad (2)$$

As the risk needs to be calculated before the next edge is known, $\Delta\chi$ is also unknown in the connection phase. With bigger $\Delta\chi$, d becomes large. To prevent d from becoming too large, $\Delta\chi$ is limited to $\frac{\pi}{2}$. Also, since the direction of the turn is not known a-priori the cross-track deviation is applied to both sides of the edge to account for both left and right hand turns. To account for possible errors during flight the minimum size of the Flight Geography as specified in SORA 2.5 Annex A [8], $3 \cdot CD$, is added. The characteristic dimension (CD) of the UAV is the largest straight line distance within the UAV's geometry, e.g. its wingspan. The resulting width of the Flight Geography is hence calculated as

$$S_{\mathrm{FG}} = 3 \cdot CD + 2 \cdot R_{\min} \cdot \left[1 - \cos\left(\frac{\pi}{4}\right)\right] \quad , \quad (3)$$

assuming that during query phase no single change of direction $\Delta\chi$ is ever larger than $\frac{\pi}{2}$.

B. Sampling the Flight Area

To create an accurate representation of the flight area the Halton sequence is used as it strikes a good balance between a uniform and random distribution without leading to sample clusters [19]. The sample density is determined by calculating the area covered by a node using the determined buffer sizes for the lowest flight speed. This sample density is then used to calculate the required number of nodes to cover the area of operation.

As narrow passages often don't get sampled, additional nodes are explicitly placed in the middle of narrow passages. Narrow passages are defined as having a width of less than five percent of the width or length of the bounding box containing the area of operation. This value needs to be tailored to the investigated area of operation. In each detected narrow passage a single additional node is placed.

Each node is then initialized with the sizes of FG, CV and GRB for the discrete speed values chosen from the UAVs flight envelope and the given height. For each speed, the equations determining the affected volumes (FG & CV) and the GRB are chosen based on the corresponding flight configuration (e.g. multirotor). This later on allows the path planner to take advantage of alleys within the flight area that can only be traversed when operating the UAV in a certain configuration and at a certain speed.

Finally, population density and air space information are analyzed for the determined GRB and CV to determine GRC and ARC, respectively, which are then combined to determine the corresponding SAIL.

C. Connection Phase

Following the attribution of the nodes, the connection phase takes place. For every straight line between two neighbouring nodes a collision check is performed for the Flight Geography. This includes collisions with obstacles, the boundaries of the area of operation as well as collisions with the digital surface model. In addition, it is checked whether the climb rate of the UAV is sufficient to surmount the altitude difference between the nodes, as each node lies at the same height above ground level (AGL). In the context of this paper it is assumed that the digital surface model is accurate enough to ensure avoiding collisions with buildings. To represent different obstacles the position of wind energy turbines and large cell towers are extracted from OpenAIP [16] and buffered with a circle with a radius of 100 m.

After performing both the collision and climb checks, the operational risk for each edge must be determined. To account for the necessary overlap between consecutive edges, semi-circles are added to both ends of the rectangular edge. This results in the shape shown in the middle of figure 4. As the risk increases with flight speed, flying below the edge's maximum allowed flight speed never exceeds the calculated risk. It is assumed that the maximum speed changes are completed within the area (circle) surrounding each node. Since these areas overlap when edges are connected, it is ensured that during a speed change, the UAV remains within the area considered during the operational risk assessment corresponding to the correct speed. After calculating the operational areas of the edge for different speeds, the respective associated SAIL are determined. Therefore each geometrical edge leads to multiple edge weights for different speeds.

A possible resulting flight path created by the combination of multiple edges is shown in figure 4. The deviation from the line of sight between nodes arises from the flight dynamic constraints, as UAVs cannot follow arbitrary flight paths and must adhere to speed-dependent curve radii. Due to the chosen width of the FG, see equation 3, flight paths stay within the FG.

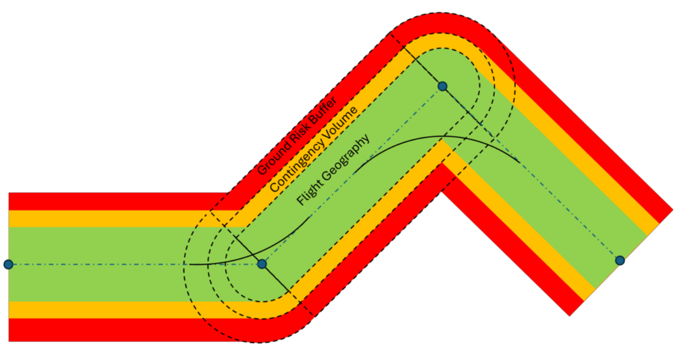

Fig. 4: Operational areas represented by graph elements

IV. Results and Discussion

Following, we demonstrate the presented framework by generating a graph for operating a UAV in Aachen. For this paper, the tilt-wing UAV *TW-Neo* is used as convertiplane, see figure 5. A tilt-wing UAV is VTOL capable by tilting its wings upward for takeoff and landing as well as hovering, thereby resembling a multicopter. For cruise flight, the wings are tilted forward such that the UAV acts like a fixed-wing aircraft.

Fig. 5: Tilt-wing UAV: TW-Neo in multirotor mode

The dimensions and flight characteristics of the TW-Neo required for the calculations of CV and GRB are summarized in table II.

TABLE II: Dimensions and flight performance characteristics of TW-NEO

Parameter	Value
Span	1.85 m
Length	1.5 m
MTOM	8 kg
Max. flight time (fixed-wing flight)	60 min
Cruise speed	25 m/s
Transition speed range	18–21 m/s
Max. bank angle ($\Phi_{\max}$)	$\pm 40°$

The UAV is considered to behave like a multirotor system below the start of the transition range, i.e. for $V < 18$ m/s. Therefore, the speed values for the risk calculation are set to 15 and 25 m/s, respectively, to cover both multirotor and fixed-wing mode.

The dimensions of Contingency Volume, Ground Risk Buffer, and Flight Geography resulting for the two different flight modes (multirotor (MR) and fixed-wing (FW)) are summarized in table III.

TABLE III: Dimensions of operational volumes for TW-Neo at different speeds

Config.	V	H_{FG}	H_{CV}	S_{CV}	S_{GRB}	S_{FG}
MR	15.0 m/s	60.0 m	80.42 m	73.67 m	61.66 m	21.56 m
FW	25.0 m/s	60.0 m	83.93 m	104.93 m	84.85 m	50.03 m

The graph of Aachen was created with a total of 2760 nodes. The number of base nodes was determined by calculating the area per node using the buffer size for the lowest speed. Applying this to one square kilometre results in a sample density of about 15 samples per square kilometre. Based on the area of Aachen this results in 2413 nodes needed to cover Aachen. Some 347 nodes were automatically added to cover narrow passages.

As mentioned before, taking into account multiple flight speeds enables the flight planner to include slower sections for short distances in order to find "shortcuts" through areas which would be of higher risk if operated at 25 m/s.

The number of nodes and edges generated are summarized in table IV. Comparing the k-PRM* approach with the PRM* approach for the connection phase shows that the k-PRM* creates more edges for the same number of nodes. In this example, k-PRM* increases the amount of edges by 255.7 % compared to the number of edges created by PRM*.

The average computation times are also shown in table IV. All computations were performed on a laptop with an Intel Core i7-1360P processor and 32 GB of RAM.

The corresponding graphs are shown in figure 6 along with obstacles (pink circles), helipad and associated airspace (black circles) and coloured edges showcasing the risk from SAIL I (white) to SAIL VI (dark red). Figure 6a depicts the graph created with the k-PRM* algorithm while figure 6b shows the graph created with the PRM* algorithm. The graph generated by k-PRM* contains significantly more edges than the one generated by PRM*. This is due to k-PRM* determining k before the connection phase, solely based on the total number of nodes and regardless of the distance between them. The different length of the edges can distort the risk representation, as the weight for the edge is always the highest risk along the edge. Therefore, a flight along an edge with 99% SAIL I and 1% SAIL V is considered riskier than a flight along an edge with 100% SAIL IV. In the graph created with the PRM* algorithm the length of the edges is limited by the connection radius, leading to fewer edges.

In the top left corner of the area of operation all figures show the effect of the narrow passage detection. In this area a wind energy turbine farm is located, resulting in many narrow passages between the wind turbines. The effect of the helipad in the lower half of figure 6a as well as the high population density to the right of the helipad can be seen in the SAIL map, for they lead to edges categorized as SAIL VI. The effect of the lower flight speed (15 m/s vs. 25 m/s) can be seen in figure 6c. As expected, the number of edges with a lower SAIL increases.

When weighing the two algorithms against each other, one must consider whether the increased number of edges is worth the increase in both computation time and graph size or if dense node placement combined with narrow passage detection and the PRM* algorithm will suffice. For Aachen, using the calculated number of 2413 nodes combined with the 347 added nodes for narrow passages results in a graph that does not have any unconnected subgraph (n-US) for the k-PRM* algorithm and one n-US for the PRM* algorithm. However, for lower number of nodes this changes drastically. The number of total nodes, resulting number of unconnected subgraphs, and number of edges are also presented in table IV. If the number of nodes gets too low the connection distance

TABLE IV: Comparison of used algorithms

Algorithm	Total nodes	Edges	n-US	Avg. comp. time
PRM*	2760	21180	1	70.476 s
PRM*	847	4522	81	26.46 s
k-PRM*	2760	75338	0	223.921 s
k-PRM*	847	16240	0	48.23 s

of the PRM* algorithm is no longer sufficient. The nodes are then too far apart to be connected, resulting in a high number

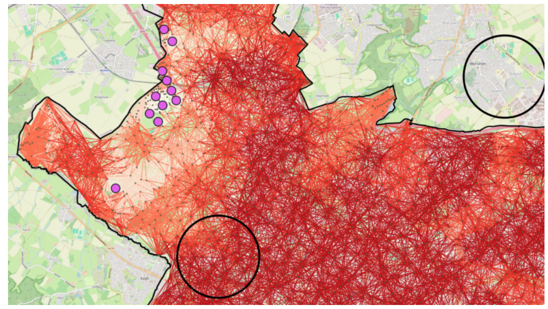

(a) Graph with 2760 nodes and 75338 edges created with the k-PRM* algorithm with k=11 and a flight speed of 25 m/s

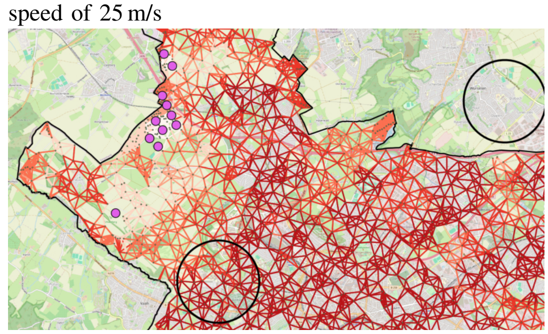

(b) Graph with 2760 nodes and 21180 edges created with the PRM* algorithm with connection radius r=412.64 m and a flight speed of 25 m/s

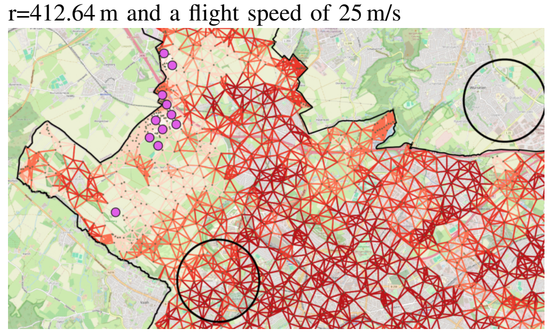

(c) Graph with 2760 nodes and 21180 edges created with the PRM* algorithm with connection radius r=412.64 m and a flight speed of 15 m/s

Fig. 6: Excerpt from the graphs of Aachen showing obstacles, air spaces and the calculated risk (SAIL) for each edge

of unconnected subgraphs. In contrast, k-PRM* still manages to connect all nodes without creating unconnected subgraphs, despite the low number of samples. In addition to the challenge of generating unconnected subgraphs, a low number of nodes results in information loss as the theoretical coverage of the node area diminishes compared to the actual area.

V. Conclusion

This paper presents a framework to generate a risk annotated graph ready to be used for flight path planning of uncrewed convertiplanes. For every edge of the graph the resulting risk levels are determined for multiple flight speeds. This enables the flight planner to trade speed for risk.

Graph generation is performed through a modified Probabilistic Roadmap algorithm. To assess the operational risk, the SORA process is applied to convertiplanes. This leads to significantly different risk levels for different flight speeds. Multiple open-source geospatial data sources are incorporated in the creation process of the risk annotated graph. Additionally, varying flight dynamic constraints are taken into account.

The result is a risk graph representation of the flight zone for the operation of a convertiplane at different air speeds. Saving SAIL information for different air speeds enables the identification of so called "shortcuts" in high-risk areas that would be avoided when considering only the cruise speed. The SAIL information is created by determining the ground risk class based on both population density and land use information and the air risk class based on airspace information.

Finally, the process is applied using two different PRM algorithm variants. When choosing between the k-PRM* and PRM* algorithms, the downside of increasing computation time to reduce the number of unconnected subgraphs by increasing the number of edges needs to be considered. To avoid creating unconnected subgraphs, it is suggested to place additional nodes in narrow passages of the flight area, and to choose a sufficient sample density based on the area per node under consideration in the risk assessment process.

A. Future Work

In the future, the graph search algorithm of the query phase for finding flight paths should be implemented. This search algorithm should not only consider operational risk but also energy consumption as frequent switching between flight speeds negatively affects the range of the UAV. Therefore, energy consumption of the UAV should be integrated into the graph, and the path planning algorithm should be adapted to consider multiple objectives.

References

[1] Interreg Meuse-Rhine, *EDEN-Medical Project*, Accessed: 2026-02-03, 2025. [Online]. Available: https://www.interregmeuserhine.eu/en/projects/eden-medical/

[2] S. Du, G. Zhong, F. Wang, B. Pang, H. Zhang, and Q. Jiao, "Safety risk modelling and assessment of civil unmanned aircraft system operations: A comprehensive review," *Drones*, vol. 8, no. 8, p. 354, Jul. 2024, ISSN: 2504-446X. DOI: 10.3390/drones8080354

[3] S. Schopferer, J. Schlapbach, G. Strickert, L. González Combrink, and S. Fendel, "Minimum Ground Risk Trajectory Planning Based On Time-Annotated Population Density Maps," en, in *AIAA SCITECH 2024 Forum*, Orlando, FL: American Institute of Aeronautics and Astronautics, Jan. 2024, ISBN: 978-1-62410-711-5. DOI: 10.2514/6.2024-0233 Accessed: Nov. 7, 2025.

[4] S. Primatesta, M. Scanavino, G. Guglieri, and A. Rizzo, "A risk-based path planning strategy to compute optimum risk path for unmanned aircraft systems over populated areas," in *2020 International Conference on Unmanned Aircraft Systems (ICUAS)*, IEEE, 2020, pp. 641–650.

[5] S. Primatesta, "A 2.5d risk-aware path planning method for safe UAS operations in populated environments," in *2024 International Conference on Unmanned Aircraft Systems (ICUAS)*, Chania - Crete, Greece: IEEE, Jun. 2024.

[6] Commission of the European Union, *Commission implementing regulation (eu) 2019/947*, 2019.

[7] EASA, *Easy Access Rules for Unmanned Aircraft Systems: Revision from September 2022*, 2022.

[8] Joint Authorities for Rulemaking on Unmanned Systems, *Specific operations risk assessment (sora) annex a*, JAR-DEL-SRM-SORA-A-2.5, 2024.

[9] F. Baader, P. Müller, A.-K. Sturm, J. Holsten, and D. Moormann, "Operational permit: Application for a tilt-wing uav according to the eu-2019-947 regulation in the specific category," in *Proceedings of the 2024 CEAS EuroGNC conference*, Bristol, UK, Jun. 2024. DOI: 10.82124/CEAS-GNC-2024-074

[10] L. Kavraki, P. Svestka, J.-C. Latombe, and M. Overmars, "Probabilistic roadmaps for path planning in high-dimensional configuration spaces," *IEEE Transactions on Robotics and Automation*, vol. 12, no. 4, pp. 566–580, Aug. 1996, ISSN: 2374-958X. DOI: 10.1109/70.508439 Accessed: Nov. 7, 2025.

[11] S. Karaman and E. Frazzoli, "Sampling-based algorithms for optimal motion planning," *The international journal of robotics research*, vol. 30, no. 7, pp. 846–894, 2011.

[12] OpenStreetMap contributors, *Planet dump retrieved from https://planet.osm.org*, https://www.openstreetmap.org, 2017.

[13] F. Batista, S. Freire, and C. Pigaiani, *Jrc-census population grid 2021*, 2024. DOI: 10.2905/98336641-FD1C-4992-8C7B-C470DD5EB81E

[14] NASA JPL, *Nasadem merged dem global 1 arc second v001*, https://doi.org/10.5069/G93T9FD9, Distributed by OpenTopography, 2021. Accessed: Feb. 4, 2026.

[15] European Environment Agency, *Eu-dem: European digital elevation model*, 2016.

[16] OpenAIP, *Open aip, free worldwide aviation database*, 2025. [Online]. Available: https://www.openaip.net/

[17] F. Batista and C. Pigaiani, *LUISA base map 2018*, en, http://data.europa.eu/89h/51858b51-8f27-4006-bf82-53eba35a142c, Accessed: 2026-2-4, Mar. 2021.

[18] EASA, *Guidelines on static population density data for the determination of the ground risk of uas operations*, Issue no.: 1, Sep. 2025.

[19] S. M. LaValle, *Planning Algorithms*, en, 1st ed. Cambridge University Press, May 2006. DOI: 10.1017/CBO9780511546877